

NEAR INFRARED COUNTERPART OF 2E 1613.5–5053 THE CENTRAL SOURCE IN SUPERNOVA REMNANT RCW 103

S. P. TENDULKAR, V. M. KASPI, R. F. ARCHIBALD, P. SCHOLZ

Department of Physics and McGill Space Institute, McGill University, 3600 University St., Montreal QC, H3A 2T8, Canada
and

National Research Council of Canada, Herzberg Astronomy and Astrophysics, Dominion Radio Astrophysical Observatory, P.O. Box 248, Penticton, BC V2A 6J9, Canada

ABSTRACT

On 2016 June 22, 2E 1613.5–5053, the puzzling central compact object in supernova remnant RCW 103, emitted a magnetar-like burst. Using Director’s Discretionary Time, we observed 2E 1613.5–5053 with the Hubble Space Telescope (WFC3/IR) and we report here on the detection of a previously unseen infrared counterpart. In observations taken on 2016 July 4 and August 11, we detect a new source ($m_{F110W} = 26.3$ AB mag and $m_{F160W} = 24.2$ AB mag) at the *Chandra* position of 2E 1613.5–5053 which was not detected in HST/NICMOS images from 2002 August 15 and October 8 to a depth of 24.5 AB mag (F110W) and 25.5 AB mag (F160W). We show that these deep IR observations rule out the possibility of an accreting binary but mimic IR emission properties of magnetars and isolated neutron stars. The presence or absence of a low-mass fallback disk cannot be confirmed from our observations.

1. INTRODUCTION

2E 1613.5–5053 was discovered as a bright X-ray source in the supernova remnant (SNR) RCW 103 using the *Einstein* X-ray Observatory (Tuohy & Garmire 1980). The nature of 2E 1613.5–5053 has been mysterious for the past three decades. With soft thermal X-ray emission, an apparent absence of radio detection, a location in the center of an SNR, it was first classified as a Central Compact Object (CCO; de Luca 2008). However, this classification is fraught with trouble. Unlike CCOs whose X-ray luminosity is usually stable, 2E 1613.5–5053 shows variations in X-ray luminosity over multiple orders of magnitudes (Gotthelf et al. 1999; Esposito et al. 2011) on timescales of months and years.

A suprising 6.67-hr periodicity was discovered with nearly 50% modulation in the X-ray band (De Luca et al. 2006) with no hint of faster pulsations. The 6.67-hr periodicity is too slow for the rotation of a young isolated neutron star, requiring exotic explanations for origins or braking mechanisms such as wind and/or disk accretion (De Luca et al. 2006; Li 2007). The periodicity is typical of compact binaries and models of tidal locking with a binary companions (Pizzolato et al. 2008) and propeller emission from an accretion disk in a pre-low mass X-ray binary (Bhadkamkar & Ghosh 2009) has been suggested to explain the periodicity as an orbital modulation. However, deep near infrared (NIR) imaging has limited any binary companion to be less massive

than an M6 star, too small to support an accretion luminosity of $10^{34-35} \text{ erg s}^{-1}$ (De Luca et al. 2008, hereafter dL08).

On 2016 June 22, the *Swift* Burst Alert Telescope (BAT, Barthelmy et al. 2005) detected a millisecond-timescale magnetar-like burst from the region of SNR RCW 103 (D’Ai et al. 2016). *Swift* slewed its X-ray Telescope (XRT, Burrows et al. 2005) and detected that 2E 1613.5–5053 was in outburst, with an absorbed 0.5–10 keV flux of $4 \times 10^{-11} \text{ erg cm}^{-2} \text{ s}^{-1}$ substantially higher than the quiescent absorbed flux of $2 \times 10^{-12} \text{ erg cm}^{-2} \text{ s}^{-1}$ in the same band. The short burst, and the double blackbody + hard power-law (spectral index $\Gamma \approx 1.2$) shape of the outburst spectrum support the source being a magnetar (D’Ai et al. 2016; Rea et al. 2016), but the origin of the 6.67-hr periodicity remains puzzling. The slowing of a magnetar via magnetic field interactions with a fallback disk was suggested and preferred by many authors but the binary scenario has not been completely ruled out (De Luca et al. 2008; D’Ai et al. 2016; Rea et al. 2016). New theoretical work suggests that a neutron star with a high magnetic field ($B \sim 5 \times 10^{15} \text{ G}$) and a fallback disk can efficiently decelerate to rotational periods of a few hours. The estimated mass of the fallback disk required to slow down the disk varies from $10^{-9} M_{\odot}$ (Ho & Andersson 2016) to $10^{-5} M_{\odot}$ (Tong et al. 2016). Whether the fallback disk survives the interaction to the present day is an unanswered question.

1.1. Near IR Counterpart/Companion

2E 1613.5–5053 lies in the Galactic plane ($l = 332^\circ, b = -0.4^\circ$) in a crowded stellar field with high extinction. This makes the identification of the counterpart or companion to 2E 1613.5–5053 challenging. Previous authors have attempted identification using photometric variability (Sanwal et al. 2002; Mignani et al. 2008) and also colors in the NIR (dL08). However, no obvious candidate has stood out from the 7 candidates in or near the 99% *Chandra* position error ellipse.

The 2016 June 22 outburst provided an opportunity to look for NIR luminosity variations that have been observed during outbursts of magnetars as well as in accretion binaries. Here we describe our Director’s Discretionary Time observations with HST/WFC3 and report a new source that was absent in the 2002 observations.

2. OBSERVATIONS & ANALYSIS

2.1. 2016 Observations

We requested DDT observations of 2E 1613.5–5053 in the F160W (*H* band) and F110W (*Y+J* band) filters using the WFC3 instrument. The images were acquired on 2016 July 4 and 2016 August 11, corresponding to 12 and 50 days after the first magnetar-like burst of 2E 1613.5–5053, respectively. The observation details are specified in Table 1. The observations were spaced to detect the likely fading of magnetars over the timescale of a month (see par. ex. Kaspi et al. 2014). However, the average X-ray luminosity of 2E 1613.5–5053 did not decrease significantly over this time period (see Section 2.3).

We used the WFC3/IR camera with a 512×512 pixel ($68'' \times 68''$) aperture in both filters. We acquired 4×321 s exposures in the F110W band and 1×105 s + 4×321 s exposures in the F160W band at both epochs. The 321-s exposures in each filter were read out using the SPARS25 sampling and the 105-s exposure was acquired using the rapid log-linear STEP25 readout to correctly image bright stars in the field¹. The exposures were dithered with the standard 4 position dither (WFC3-IR-DITHER-BOX-MIN) to improve the sampling of the point spread function (PSF) and to identify and remove cosmic rays.

We processed the images with the standard STSDAS analysis package in IRAF. We dedistorted and combined the images to a platescale of 55 mas per pixel in the F160W filter and 37.8 mas per pixel in the F110W filter using the drizzlepac package. We chose the platescales to sample the point spread function (PSF) in each filter with 2.5 pixels.

2.2. 2002 Observations

We downloaded archival NICMOS NIC2 images of 2E 1613.5–5053 acquired in 2002 August and October from

the Space Telescope Archive (Program 9467). The details of the data are specified in Table 1. The F110W images from 2002 were shallow (total exposure of 1870 s) and only the brightest stars were visible. Hence we only consider the 2002 F110W images to measure upper limits in the analysis. We did not use the F205W (*K*) band images in this analysis as they were discussed in dL08.

The image files from the August and October observations were separately dedistorted and combined using MultiDrizzle to the same plate scales and settings as the WFC3/IR observations.

2.3. Swift-XRT Observations

As the IR luminosity of magnetars may vary with the X-ray luminosity, we analyzed the 0.5–10 keV X-ray data from *Swift*-XRT observations closest in time to the 2016 HST observations. We created the *Swift*-XRT spectrum for 2E 1613.5–5053 from observations 00700791011 (2.1 ks exposure at 2016 July 4 13:21 UT) and 00030389037 (2.7 ks exposure at 2016 August 10 01:08 UT) using the automated XRT data analysis tool² (Evans et al. 2009). We fit the spectra with an absorbed blackbody model over 0.5–10.0 keV using XSPEC v12.9.0n (Arnaud 1996). We used the wilm abundance model (Wilms et al. 2000) and bcmc photoelectric cross sections (Balucinska-Church & McCammon 1992). The best fit photoelectric column density was $N_H = 1.4 \pm 0.7 \times 10^{21} \text{ cm}^{-2}$. The measured blackbody temperatures and unabsorbed fluxes were $kT_1 = 0.56 \pm 0.04 \text{ keV}$, $kT_2 = 0.60 \pm 0.3 \text{ keV}$ and $F_{X,1} = 4.5 \pm 0.4 \times 10^{-11} \text{ erg cm}^{-2} \text{ s}^{-1}$ and $F_{X,2} = 4.7 \pm 0.4 \times 10^{-11} \text{ erg cm}^{-2} \text{ s}^{-1}$, where the subscripts 1 and 2 refer to the July and August epochs, respectively. Thus, we conclude that the X-ray flux did not decrease significantly between our HST observation epochs, consistent with the X-ray light curve reported by D’Ai et al. (2016) and Rea et al. (2016).

Table 1. HST Observations of 2E 1613.5–5053.

Obs ID	Start — End (UT)	Inst/Filt ^a	Exp ^b
2016 August			
ID4V02VJQ	2016-08-11 02:48 — 02:50	WFC3/F160W	105.5
ID4V02020	2016-08-11 02:56 — 04:16	WFC3/F160W	1287
ID4V02010	2016-08-11 02:50 — 04:10	WFC3/F110W	1287
2016 July			
ID4V01B3Q	2016-07-04 02:48 — 02:50	WFC3/F160W	105.5
ID4V01020	2016-07-04 02:56 — 04:16	WFC3/F160W	1287
ID4V01010	2016-07-04 02:50 — 04:10	WFC3/F110W	1287

Table 1 continued

¹ See the instrument handbook for details: <http://www.stsci.edu/hst/wfc3>

² http://www.swift.ac.uk/user_objects/

Table 1 (*continued*)

Obs ID	Start — End (UT)	Inst/Filt ^a	Exp ^b
2002 October (archival)			
N8C501010	2002-10-08 02:26 — 04:10	NIC2/F160W	2590.5
N8C501020	2002-10-08 04:10 — 06:04	NIC2/F160W	2590.5
N8C501030	2002-10-08 06:05 — 09:09	NIC2/F160W	2590.5
N8C501040	2002-10-08 09:10 — 11:12	NIC2/F160W	2590.5
N8C501050	2002-10-08 11:13 — 12:39	NIC2/F110W	935
2002 August (archival)			
N8C502020	2002-08-15 10:28 — 12:03	NIC2/F160W	2590.5
N8C502040	2002-08-15 13:40 — 14:31	NIC2/F160W	2590.5
N8C502050	2002-08-15 15:19 — 15:41	NIC2/F110W	935
N8C502030	2002-08-15 12:04 — 12:55	NIC2/F160W	2590.5
N8C502010	2002-08-15 08:50 — 10:27	NIC2/F160W	2590.5

^a Instrument and Filter: WFC3 – Wide Field Camera 3 / IR, NIC2 – NICMOS Camera 2.

^b Exposure time in seconds.

3. RESULTS

3.1. PSF Fitting

For accurate photometry and astrometry, we performed PSF fitting on each image using the IDL code *StarFinder* (Diolaiti et al. 2000). We used a 95×95 pixel PSF model ($5.2''$ in F160W and $3.6''$ in F110W) to account for the diffraction spikes. We assumed the PSF model to be static over each drizzled image.

For each image, we used fifteen bright stars in the image to create a model PSF that was fit to all the stars in the image. This step was iterated twice and we ensured that the PSF model was cleaned of contaminating stars. We extracted the pixel coordinates and fluxes of stars in each filter and epoch. We limited the search to sources that were detected with a signal to noise ratio (SNR) greater than 3 and where the normalized PSF fitting correlation was greater than 0.8. The residual images were analysed by eye to verify that no under-fitting or over-fitting had occurred. The PSF model created for each image was saved.

We used the 2016 July F160W image as the reference for matching all objects from other images. We first corrected the world coordinate system of the reference image to the 2MASS star positions (Skrutskie et al. 2006) using the IRAF task *ccmap*. The residual fitting error was $0.11''$ (root-mean-square). Before fitting, we removed 2MASS sources that corresponded to unresolved stars in the HST images. The positions of stars in other images were matched and transformed to the image coordinate system of 2016 July F160W image using the *geomap* and *geoxytran* IRAF tasks. The residuals of the matching were ≈ 0.4 pix (22 mas). We matched the detected sources using a search radius

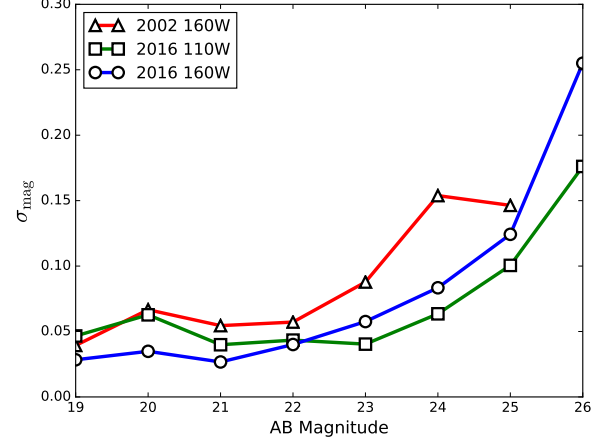


Figure 1. $1\text{-}\sigma$ scatter in photometry for the 2016 WFC3 F110W (squares), F160W (circles) and 2002 NICMOS F160W images (triangles). The scatter is due to a combination of PSF modelling errors, PSF variation over the image, background contribution and the Poisson noise. The 2002 NICMOS F110W images did not have sufficiently many stars to accurately estimate the standard deviation in each magnitude bin.

of 0.5 pixels and produced a combined list of sources and fluxes/non-detections.

3.2. Photometry

The flux reported by *StarFinder* is the integrated flux under the normalized PSF. We converted the flux to AB magnitudes using the *PHOTFNU* keyword based on the WFC3/IR and NICMOS calibration. While *StarFinder* reports a formal flux error for each star, this does not account for the error in PSF estimation, PSF variation over the image and the background estimation. We estimated the scatter in fluxes by comparing the fluxes measured in the 2016 July images to 2016 August images and 2002 August images to the 2002 October images. As the image pairs were acquired with the same instrumental configuration separated only by a few months, the scatter in the fluxes should be dominated by the errors arising from the sources discussed above.

Figure 1 shows the measured magnitudes and magnitude differences in the pairs of images and the calculated scatter in 1 mag bins. The NICMOS F110W images were not used for this analysis as they did not have sufficient stars to accurately estimate the standard deviation in each magnitude bin. Comparing the photometry between WFC3 and NICMOS, we find that the faint star (> 20 mag) photometry matches within errors and there is no significant zeropoint difference. The bright star photometry with NICMOS is known to have a non-linearity³ and it is detectable at a 0.1 mag level for bright stars.

³ <http://www.stsci.edu/hst/nicmos/performance/anomalies/nonlinearity.html>

3.3. Detected Sources

We labeled the sources detected in the field as per the scheme used in [dL08](#) (Figure 2). We detected a new object, Source 8, in the 2016 images inside the *Chandra* position ellipse. The magnitudes of the source along with photometric scatter (as calculated above) are given in Table 2.

Source 8 was not detected in the 2002 images (Figure 3, left panel). As a verification, we converted the measured F160W flux from the 2016 July measurement into the expected NICMOS count rate. Using the PSF extracted from

the 2002 August and 2002 October images, we injected a fake source at the location of source 8. The source is clearly visible and also detected by the same analysis pipeline as utilized above (Figure 3, middle panel). By reducing the brightness of the injected source till it was not detected in our analysis pipeline, we estimate the limiting brightness of source 8 in 2002 August and 2002 October (Table 2). We put $3\text{-}\sigma$ upper limits of $m_{\text{F110W}} > 24.5$ and $m_{\text{F160W}} > 25.2$ for individual images. If the 2002 August and October images are combined, the limiting magnitudes are $m_{\text{F110W}} \gtrsim 25$ and $m_{\text{F160W}} \gtrsim 25.5$.

Table 2. Photometry of sources near the location of 2E 1613.5–5053.

#	2002				2016			
	Aug		Oct		Jul		Aug	
	m_{F110W}	m_{F160W}	m_{F110W}	m_{F160W}	m_{F110W}	m_{F160W}	m_{F110W}	m_{F160W}
1	23.8 ± 0.2	21.20 ± 0.06	23.8 ± 0.2	21.16 ± 0.06	23.84 ± 0.07	21.44 ± 0.04	23.76 ± 0.07	21.40 ± 0.04
2 ^a	19.1 ± 0.1	18.02 ± 0.04	19.1 ± 0.1	18.01 ± 0.04	19.70 ± 0.06	18.37 ± 0.03	19.63 ± 0.06	18.38 ± 0.03
3	> 24.5	22.92 ± 0.09	> 24.5	22.91 ± 0.09	25.55 ± 0.15	23.04 ± 0.06	25.45 ± 0.15	23.05 ± 0.06
4	> 24.5	22.50 ± 0.08	> 24.5	22.61 ± 0.08	25.53 ± 0.14	22.90 ± 0.06	25.65 ± 0.15	23.04 ± 0.06
5	> 24.5	23.19 ± 0.11	> 24.5	23.20 ± 0.11	26.51 ± 0.21	23.53 ± 0.07	26.19 ± 0.20	23.51 ± 0.07
6	> 24.5	23.25 ± 0.11	> 24.5	23.20 ± 0.11	26.45 ± 0.21	23.50 ± 0.07	26.26 ± 0.20	23.46 ± 0.07
7	> 24.5	22.96 ± 0.09	> 24.5	22.94 ± 0.09	25.37 ± 0.12	23.11 ± 0.06	25.26 ± 0.12	23.09 ± 0.06
8 ^b	> 24.5	> 25.2	> 24.5	> 25.2	26.27 ± 0.20	24.24 ± 0.08	26.39 ± 0.21	24.51 ± 0.10

NOTE—All magnitudes are measured in the AB magnitude scale.

^a Star 2 is affected by the photometric nonlinearity of the NICMOS detector and hence the difference in 2002 and 2016 magnitudes is not astrophysical.

^b New source detected only in 2016 observations.

4. DISCUSSION

Following the 2016 magnetar flare and X-ray brightening of 2E 1613.5–5053, we have detected a new infrared source at the X-ray location of 2E 1613.5–5053. The infrared source brightened by at least 1.3 mag (F160W) compared to the non-detections in previous 2002 observations. Thus, we conclude that this source is associated with 2E 1613.5–5053 and we discuss the implications, and the physical scenarios for explaining its 6.67-hr X-ray modulation.

Dust Extinction in IR— To interpret the nature of the source, we must first try to determine its intrinsic brightness, corrected for extinction. The magnitude of the optical/IR extinction towards 2E 1613.5–5053 is uncertain. The dust maps of [Schlafly & Finkbeiner \(2011\)](#) estimate $A_V = 36$ mag in the direction of 2E 1613.5–5053⁴. This is also supported by the average $H - K$ color of the surrounding stars from [dL08](#)

who estimate $A_V = 20 - 40$ for the whole field. However, the near-IR spectroscopy of RCW 103 ([Oliva et al. 1989](#)) and the photoelectric absorption column density (N_H) estimated from X-ray observations of 2E 1613.5–5053 and RCW 103 ([Foight et al. 2016](#)) suggest a much lower value of $A_V = 3 - 6$.

Here, we discuss both the high extinction case ($A_V = 36$ mag) and the low extinction case ($A_V = 3.5$ mag) assuming the distance of 3.3 kpc to RCW 103 ([Tuohy & Garmire 1980](#)) but we consider that the low extinction value is substantially more likely since it arises from measurements of 2E 1613.5–5053 and RCW 103 themselves. We also show that the high extinction case leads to infeasible scenarios.

For each case, we discuss whether the IR emission could be due to a companion/accretion disk (binary scenario) in which case the 6.67-hr period could be interpreted as the orbital period. We also discuss, alternatively, whether the IR emission is from the neutron star or a fallback disk (isolated scenario) where the 6.67 hr period is interpreted as the rotational period of the neutron star.

The 0.5–10 keV X-ray flux at the 2002 and 2016 ob-

⁴ <http://irsa.ipac.caltech.edu/applications/DUST/>

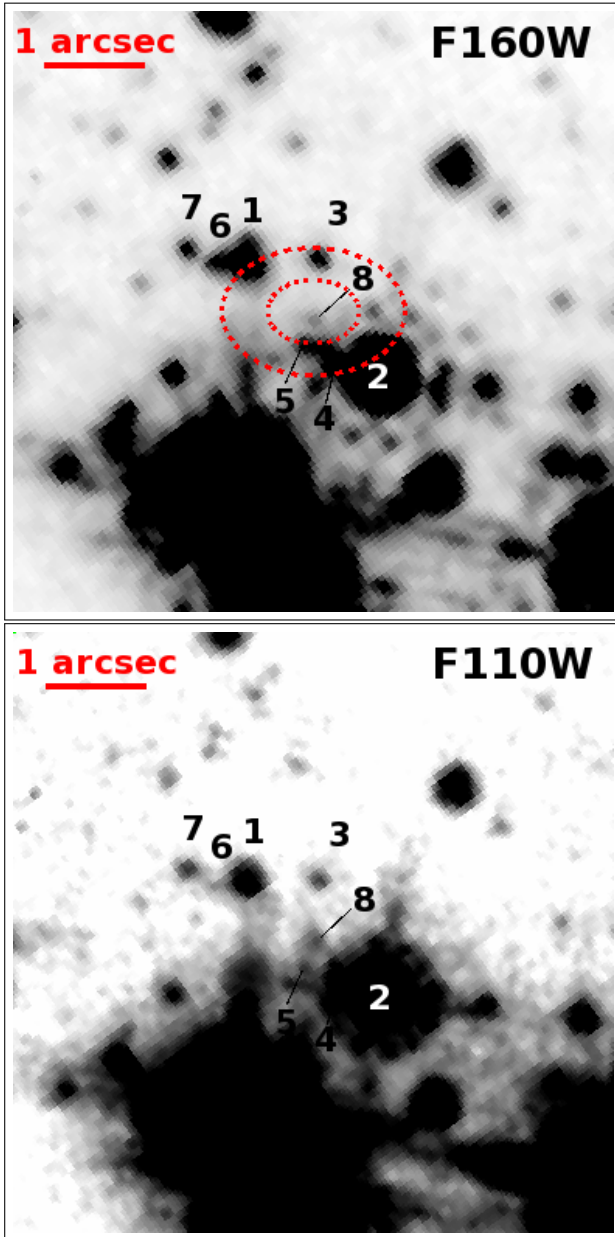


Figure 2. WFC3 F160W (top panel) and F110W (bottom panel) images of 2E 1613.5–5053 from July 2016. The stars are labelled as per dL08 and the new detection, source 8 is marked. The dotted ellipse shows the 68% and 99% position error ellipse calculated by dL08.

servation epochs was approximately $6 \times 10^{-12} \text{ erg cm}^{-2} \text{ s}^{-1}$ (dL08) and $4.5 \times 10^{-11} \text{ erg cm}^{-2} \text{ s}^{-1}$ (Rea et al. 2016), respectively. This corresponds to intrinsic luminosities of $L_X = 7 \times 10^{33} \text{ erg s}^{-1}$ and $L_X = 5 \times 10^{34} \text{ erg s}^{-1}$, an increase by a factor of ~ 7 .

4.1. High Extinction Case

If $A_V = 36 \text{ mag}$, the extinction in the F110W and F160W bands is 9.5 mag and 6.0 mag, respectively. Thus, including a distance modulus of $5 \log(3.3 \text{ kpc}/10 \text{ pc}) = 12.6 \text{ mag}$, the absolute AB magnitudes of source 8 in 2016 are 4.2 (F110W) and 5.6 (F160W). The corresponding limits in 2002

are > 2.4 , and $> 6.9 \text{ AB mag}$, respectively.

We compared the absolute magnitudes to stellar spectrophotometry (Cox 2000, Table 15.7) and white dwarf models (Tremblay et al. 2011; Bergeron et al. 2011, and references therein⁵). The 2002 NICMOS upper limits are consistent with main-sequence stars cooler than M2 or with DA and DB white dwarfs as companions to 2E 1613.5–5053. However, dL08 used deeper K_s band VLT upper limits to rule out any binary companions brighter than a M6–M8 dwarf. Also, the F110W–F160W color of -1.4 in the 2016 observations is bluer than blackbodies of 10^{15} K , ruling out any interpretation of the infrared flux as blackbody emission from a star or an accretion disk. Interpreting the color as power-law emission (ν^α), we get $\alpha \approx 4.5$, rising far steeply than the observed spectra from low mass X-ray binary accretion disks ($0.5 \lesssim \alpha \lesssim 1.5$) (Hynes 2005).

The 2016 IR luminosity of 2E 1613.5–5053 corresponds to $L_{F110W} = 10^{33} \text{ erg s}^{-1}$ and $L_{F160W} = 2 \times 10^{32} \text{ erg s}^{-1}$. Comparing the IR and X-ray luminosities, we get $L_X/L_{F110W, F160W} \approx 50 - 200$. This ratio of X-ray to IR luminosities is also significantly lower than the values of 10^4 observed for isolated neutron stars, magnetars and CCOs (Fesen et al. 2006; Wang et al. 2006; Mignani et al. 2008).

Thus, we find that the high extinction scenario leads to astrophysically infeasible cases and we do not discuss it further.

4.2. Low Extinction Case

If $A_V = 3.6$, the extinction in the F110W and F160W bands is 0.9 mag and 0.6 mag, respectively. This leads to absolute AB magnitudes in 2016 of 12.8 (F110W) and 11.0 (F160W). The corresponding 2002 upper limits are $> 11.0 \text{ AB mag}$ and $> 12.3 \text{ AB mag}$, respectively.

For a companion object, the 2002 upper limits are inconsistent with the coolest M-dwarfs. The absolute magnitudes of very compact cooler white dwarfs are consistent with this non-detection. However, a white dwarf companion in an LXMB must necessarily form after the neutron star and hence must be younger than the neutron star or the supernova remnant. Among white dwarfs younger than 2 kyr, only the compact hydrogen atmosphere (DA) white dwarfs (surface gravity $\log g \gtrsim 9.5$) are consistent with the F160W and F110W upper limits from 2002. The high $\log g$ implies a mass of $\sim 1.3 M_\odot$ for C, O and mixed CO cores (Fontaine et al. 2001) and a very tiny radius of $\lesssim 5000 \text{ km}$. This radius is much smaller than the orbital radius ($1.7 \times 10^6 \text{ km}$) for a $1.3 M_\odot$ white dwarf orbiting with a $1.4 M_\odot$ neutron star with a 6.67-hr period and the corresponding Roche lobe radius. Hence such a white dwarf could not provide the accretion power for the X-ray luminosity.

The F110W and F160W luminosities are $L_{F110W} = 4 \times$

⁵ <http://www.astro.umontreal.ca/~bergeron/CoolingModels>

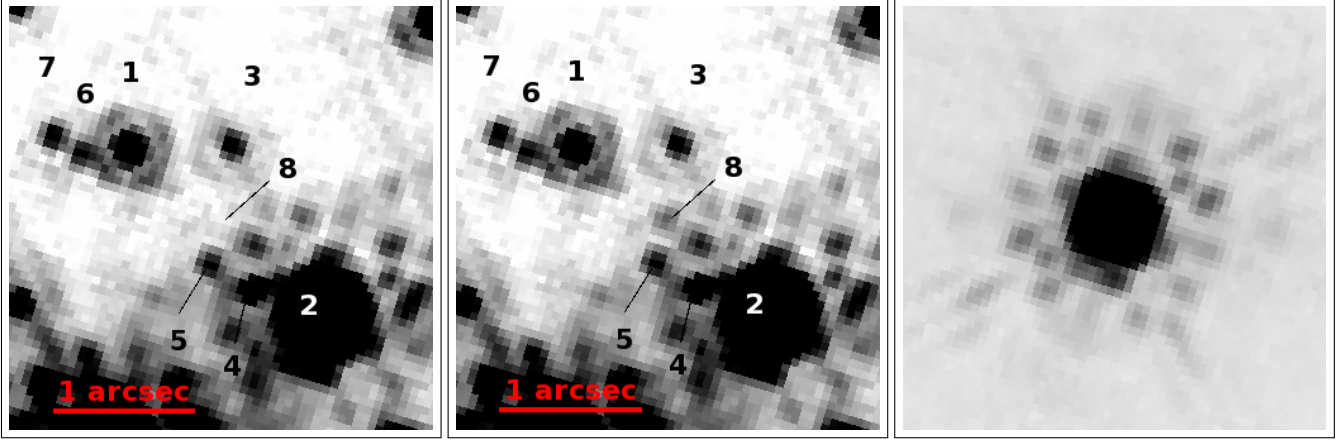


Figure 3. Verifying the detectability of source 8 in 2002 F160W images. *Left Panel:* Original 02-J-160 image. *Middle Panel:* 02-J-160 image with source 8 injected by scaling the extracted PSF (*right panel*) to an AB magnitude of 24.2 mag. The source is easily detected. The bright spots to the lower right of source 8 in the middle panel are speckles of the PSF as shown in the right panel.

$10^{29} \text{ erg s}^{-1}$ and $L_{\text{F160W}} = 7 \times 10^{29} \text{ erg s}^{-1}$. The corresponding X-ray to IR fluence ratios $L_X/L_{\text{F110W}, \text{F160W}} \approx 10^5$ are consistent with those of magnetars such as 4U 0142+61 (Hulleman et al. 2004), 1E 1048.1–5937 (Tam et al. 2008) and limits on other magnetars (Fesen et al. 2006; Wang et al. 2006; Mignani et al. 2008). It is not clear, however, whether this emission arises from the magnetosphere of the neutron star or whether it arises from a fallback disk, as has been suggested around 4U 0142+61 (Wang et al. 2006) and 1E 2259+586 (Kaplan et al. 2009). Wang et al. (2007) measured *Spitzer* flux upper limits to be 10^{-4} Jy ($4.5 \mu\text{m}$) and $3 \times 10^{-4} \text{ Jy}$ ($8 \mu\text{m}$). These measurements do not rule out the presence of a disk as massive as the one around 4U 0142+61 ($10 M_{\oplus} = 6 \times 10^{28} \text{ g}$). Indeed, the amount of material required to slow down the magnetar to its current period is tiny — Ho & Andersson (2016) estimate it to be 10^{24} g while Tong et al. (2016) estimate the mass to be 10^{28} g .

Thus, while the presence or absence of a fallback disk cannot be confirmed at this point, we have shown that the binary scenarios for the evolution of 2E 1613.5–5053 can be ruled out with a high level of confidence. Further understanding of the nature of 2E 1613.5–5053 can be achieved via spectroscopy of the faint IR source to search for disk emission features and whether the continuum is better described by a power law spectrum or a disk blackbody spectrum. While

this is extremely challenging with current observational capabilities, it may be possible with the James Webb Space Telescope.

The authors thank the Hubble Space Telescope operations teams for their speed and flexibility scheduling these observations.

Based on observations made with the NASA/ESA Hubble Space Telescope, obtained from the Data Archive at the Space Telescope Science Institute, which is operated by the Association of Universities for Research in Astronomy, Inc., under NASA contract NAS 5-26555. These observations are associated with programs #9467 and #14814. This work also made use of data supplied by the UK Swift Science Data Centre at the University of Leicester.

S.P.T acknowledges support from a McGill Astrophysics postdoctoral fellowship. V.M.K. receives support from an NSERC Discovery Grant, an Accelerator Supplement and from the Gerhard Herzberg Award, an R. Howard Webster Foundation Fellowship from the Canadian Institute for Advanced Study, the Canada Research Chairs Program, and the Lorne Trottier Chair in Astrophysics and Cosmology. R.F.A. acknowledges support from an NSERC CGSD. P.S. received support from a Schulich Graduate Fellowship from McGill University and holds a Covington Fellowship at DRAO.

REFERENCES

- Arnaud, K. A. 1996, in *Astronomical Society of the Pacific Conference Series*, Vol. 101, *Astronomical Data Analysis Software and Systems V*, ed. G. H. Jacoby & J. Barnes, 17
- Balucinska-Church, M., & McCammon, D. 1992, *ApJ*, 400, 699
- Barthelmy, S. D., Barbier, L. M., Cummings, J. R., et al. 2005, *SSRv*, 120, 143
- Bergeron, P., Wesemael, F., Dufour, P., et al. 2011, *ApJ*, 737, 28
- Bhadkamkar, H., & Ghosh, P. 2009, *A&A*, 506, 1297
- Burrows, D. N., Hill, J. E., Nousek, J. A., et al. 2005, *SSRv*, 120, 165
- Cox, A. N. 2000, *Allen’s Astrophysical Quantities*
- D’Ai, A., Evans, P. A., Gehrels, N., et al. 2016, *The Astronomer’s Telegram*, 9180
- D’Ai, A., Evans, P. A., Burrows, D. N., et al. 2016, *ArXiv e-prints*, arXiv:1607.04264
- de Luca, A. 2008, in *American Institute of Physics Conference Series*, Vol. 983, *40 Years of Pulsars: Millisecond Pulsars, Magnetars and More*, ed. C. Bassa, Z. Wang, A. Cumming, & V. M. Kaspi, 311–319
- De Luca, A., Caraveo, P. A., Mereghetti, S., Tiengo, A., & Bignami, G. F. 2006, *Science*, 313, 814
- De Luca, A., Mignani, R. P., Zaggia, S., et al. 2008, *ApJ*, 682, 1185
- Diolaiti, E., Bendinelli, O., Bonaccini, D., et al. 2000, *A&AS*, 147, 335

- Esposito, P., Turolla, R., de Luca, A., et al. 2011, *MNRAS*, 418, 170
- Evans, P. A., Beardmore, A. P., Page, K. L., et al. 2009, *MNRAS*, 397, 1177
- Fesen, R. A., Pavlov, G. G., & Sanwal, D. 2006, *ApJ*, 636, 848
- Foight, D. R., Güver, T., Özel, F., & Slane, P. O. 2016, *ApJ*, 826, 66
- Fontaine, G., Brassard, P., & Bergeron, P. 2001, *PASP*, 113, 409
- Gotthelf, E. V., Petre, R., & Vasisht, G. 1999, *ApJL*, 514, L107
- Ho, W. C. G., & Andersson, N. 2016, *ArXiv e-prints*, arXiv:1608.03149
- Hulleman, F., van Kerkwijk, M. H., & Kulkarni, S. R. 2004, *A&A*, 416, 1037
- Hynes, R. I. 2005, *ApJ*, 623, 1026
- Kaplan, D. L., Chakrabarty, D., Wang, Z., & Wachter, S. 2009, *ApJ*, 700, 149
- Kaspi, V. M., Archibald, R. F., Bhallerio, V., et al. 2014, *ApJ*, 786, 84
- Li, X.-D. 2007, *ApJL*, 666, L81
- Mignani, R. P., Zaggia, S., Dobrzycka, D., et al. 2008, in *American Institute of Physics Conference Series*, Vol. 983, 40 Years of Pulsars: Millisecond Pulsars, Magnetars and More, ed. C. Bassa, Z. Wang, A. Cumming, & V. M. Kaspi, 325–327
- Oliva, E., Moorwood, A. F. M., & Danziger, I. J. 1989, *A&A*, 214, 307
- Pizzolato, F., Colpi, M., De Luca, A., Mereghetti, S., & Tiengo, A. 2008, *ApJ*, 681, 530
- Rea, N., Borghese, A., Esposito, P., et al. 2016, *ArXiv e-prints*, arXiv:1607.04107
- Sanwal, D., Garmire, G. P., Garmire, A., Pavlov, G. G., & Mignani, R. 2002, in *Bulletin of the American Astronomical Society*, Vol. 34, American Astronomical Society Meeting Abstracts #200, 764
- Schlaflly, E. F., & Finkbeiner, D. P. 2011, *ApJ*, 737, 103
- Skrutskie, M. F., Cutri, R. M., Stiening, R., et al. 2006, *AJ*, 131, 1163
- Tam, C. R., Gavril, F. P., Dib, R., et al. 2008, *ApJ*, 677, 503
- Tong, H., Wang, W., Liu, X. W., & Xu, R. X. 2016, *ArXiv e-prints*, arXiv:1608.02113
- Tremblay, P.-E., Bergeron, P., & Gianninas, A. 2011, *ApJ*, 730, 128
- Tuohy, I., & Garmire, G. 1980, *ApJL*, 239, L107
- Wang, Z., Chakrabarty, D., & Kaplan, D. L. 2006, *Nature*, 440, 772
- Wang, Z., Kaplan, D. L., & Chakrabarty, D. 2007, *ApJ*, 655, 261
- Wilms, J., Allen, A., & McCray, R. 2000, *ApJ*, 542, 914